



Simulation and experimental study on magnetic separation of Au loaded biomass from wastewater

Song Huiping^a, Cheng Huaigang^{a,*}, Li Xingang^b, Cheng Fangqin^{a,*}

^a*Institute of Resources and Environmental Engineering, Shanxi University, Taiyuan 030006, China
Tel./Fax: +86(351)7016893; email: huaigangcheng@yahoo.com.cn*

^b*School of Chemical Engineering and Technology, Tianjin University, Tianjin 300072, China*

Received 6 July 2011; Accepted 15 December 2011

ABSTRACT

Magnetotactic bacterium has the characteristics of both magnetotaxis and adsorbing the precious metal ions, which makes it possible to recycle the precious metal from wastewater in the combination of high gradient magnetic separation. Nickel wires were used as media which producing gradient magnetic field to separate the magnetotactic bacteria (MTB) which had adsorbed Au(III) with high gradient magnetic field from wastewater. The magnetic separation model including the material balance equation and the separation rate equation were developed to describe this process. The movement process of metal loaded bacteria in magnetic field was investigated both experimentally and theoretically. The magnetic separator developed by our research team used for separating Au loaded biomass showed high separation efficiency, with nearly 100% biomass removed at the magnetic intensity of 1200 GS in 100 min. Experimental and simulation results all showed that the trapped bacteria were deposited in multi-layers, implying the ability of multi-layer trapping for the wires. Simulation mode was in good agreement with experiments results, which meant it could be used in the future research of MTB magnetic process.

Keywords: Kinetics; Bio-magnetic separation; Simulation ; High Gradient Magnetic Separation; Gold; Magnetotactic bacterium

1. Introduction

The application of bio-sorption in the metal recycling from wastewater has always been focused [1–3]. Among the bio-adsorbents, the MTB containing Fe_3O_4 [4,5] show both ideal adsorbability to metal ions and unique characteristic of magnetotaxis. Such bacteria can carry metal ions out of wastewater with an outer magnetic field, and then naturally avoid the problem that it is not easy to leave from wastewater for many other bio-adsorbents.

The combination of the magnetic separation and bio-sorption technology was firstly reported by Bahaj et al. [6]. The high gradient magnetic separation (HGMS) technology could rapidly separate the magnetic particles, which enabled the extraction of trace metal from the wastewater. However, the weak magnetism of metal ions in the wastewater restricted the application of this technology. Then, Bahaj et al. used MTB to adsorb the metal ions and found the particles (MTB combined with metal ions) experienced obvious increase in magnetic susceptibility. Therefore, the particles could be separated from wastewater using the HGMS equipment, so

*Corresponding authors.

that the metals could be extracted. Our previous works [7,8] have also proved that MTB could quickly adsorb the Au(III) in the wastewater and the adsorption efficiency could reach over 90%. And under the driven of external magnetic field, the metal-loaded MTB could move along the magnetic line and be caught by nickel wire, then be separated from the wastewater.

The researches on MTB in the application of water treatment were mostly focused on the experimental investigation of new technological process, and the mechanism of magnetic separation and computer simulation might seem to be further needed in the future exploration. Delightfully, fruitful results have been obtained in the area of magnetic separation theory, which provided important references for MTB bio-magnetic separation. It has been proved that the magnetite can separate some hazardous species and heavy metals from aqueous solutions [9], like the behavior of MTB containing Fe_3O_4 . Among the magnetic separation models, the category of single cylinder medium trapping particles has been most completely investigated, including the force equilibrium model and the tracking model [10,11]. Then the multi-cylinder trapping model has also been developed. Tsouris et al. [12] studied the prediction of the removal efficiency of paramagnetic colloidal particles by a trajectory model. Their central idea lay in the effect of the composition of gravitational, magnetic and drag forces on the magnetic particles, and the model can simulate this case well when the magnetic force overwhelmed the other two. Chen et al. [13] described the feasibility of a portable HGMS separator built from parallel tubing-wire units to efficiently sequester magnetic spheres from the blood stream, and investigated the capture efficiency of a HGMS separator unit using 2D mathematical modeling. In Chen's model, the magnetic separator was modeled as multiple arrays of parallel wires and small tubing immersed in an externally applied homogeneous magnetic field, and the basic unit was described as two ferromagnetic wires running parallel and opposite to each other along a centrally located capillary tube. Further, the 3D model [14] was also developed to analyze the effect of the separator configurations on the efficiency of magnetic sphere capture, and configuration characterized by bi-directionally alternating wires and tubes was found to be an optimal design.

Actually, the HGMS technology has been applied in many areas [15,16], for example, kaolin decolorization, enrichment of ores-mineral beneficiation, metal removal from wastewater, food processing, even protein and DNA purification. At present, the theoretical HGMS models are generally based on the initial separation state, reflecting the phenomenon of particles trapped onto the clear magnetic medium. As to the HGMS process of MTB onto nickel multi-wires [8], the magnetic

medium (nickel wires) could quickly trapped certain MTB particles, and the trapped MTB particles would affect the motion state of the whole fluid and the distribution of external force field, resulting in the increasing complexity of the description of the particles motion, so this trapping process was believed to needed further investigation.

It may be interesting to research the wastewater treatment containing heavy metal ions, Au(III), by using external magnetic field and MTB. Generally, several methods can be used for recovering metal from the waste, such as leaching, extraction, ion exchange and active carbon adsorption. Compared with these methods, bio-adsorption has the advantage of efficiently processing low concentration of metal-bearing wastewater, harmless and little secondary pollution. Especially, among a variety of bio-adsorbents, easy coupling with magnetic separation makes MTB attractive to researchers. For the magnetic separation using MTB, most of the literatures were based on experimental. Furthermore, for the practicality of this technology, theoretical knowledge of the transmission characteristics of the process is necessary. Accordingly, the objective of this article was to study both theoretically and experimentally the effects of operating conditions (magnetic intensity, initial concentration and velocity of inlet water, etc.) on the actual performance of such a bio-magnetic separation. Besides, the mathematical model, describing the motion behavior of the magnetic particles, Au-loaded MTB, in the magnetic field, was established to study the kinetics of the trapping process.

2. Experimental

The main device for separation was the magnetic separator, which showed in Fig. 1. Two permanent magnets (material is NdFeB, 1500 Gs in surface magnetic

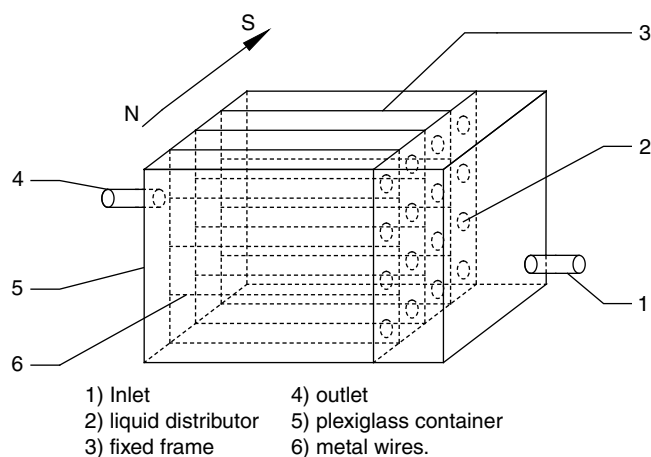


Fig. 1. Schematic diagram of magnetic separator.

intensity) were fixed on the both sides of the separator. Multi-level of metal wires (material was 50NiFe) were distributed in the separator along the flow direction. The MTB were used to adsorb the Au(III) from the feed solution, then the solution with metal-loaded MTB were driven into the magnetic separator by a peristaltic pump. The magnetic intensity was adjusted by changing the distance between the two magnets, and the Tesla-meter (model T-6) was used to detect the external magnetic intensity between $0 \approx 1200$ Gs. The experimental method had been described in the earlier paper [8].

3. Modelling of the separation process

The detailed experimental process has been described in the literature [8]. The magnetic separation model could be consisted by material balance and separation rate equations.

3.1. Material balance equation

As shown in Fig. 2, it was considered a unit with δx in length and A in lateral area in the separator, which contained a volume $A \cdot N \cdot \delta x$ of retained particles and a volume $A \cdot \epsilon C \cdot \delta x$ of moving particles entrained by the liquid; where ϵ was the porosity of MTB-loaded metal wires, C the particle mass content in fluids, N the adsorbed particle mass for each unit volume of magnetic separator.

The general mass balance equation was “accumulation rate = (flow in) – (flow out)” [17], that is:

$$\frac{\partial}{\partial t} [A(N + \epsilon C)] + \frac{\partial}{\partial x} [A u_0 C - A D \frac{\partial C}{\partial x}] = 0 \quad (1)$$

where u_0 was the velocity of inlet flow, $u_0 C$ the barycentric flow of particles entrained by the fluid, t the operating time, x the horizontal distance from the start of the wires, $-D \frac{\partial C}{\partial x}$ the diffusion flux.

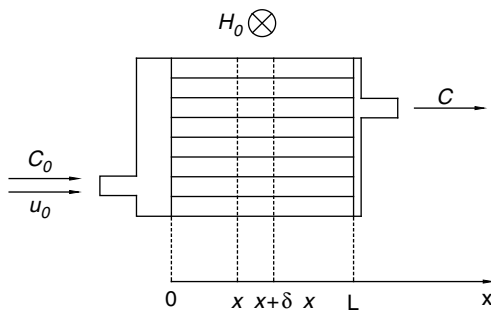


Fig. 2. The state of particle suspended liquid through the magnetic separator.

The suspension flow rate was usually kept constant. Consequently the material balance equation was as follows:

$$u_0 \frac{\partial C}{\partial x} + \frac{\partial (N + \epsilon C)}{\partial t} - D \frac{\partial^2 C}{\partial x^2} = 0 \quad (2)$$

The porosity of clean metal wires was ϵ_0 . The Eqs. (1) and (2) derived from the phenomenological model for high-gradient magnetic separation, in which some simplification modes could be considered [17]. Particles diffusion is usually negligible when their size is larger than $1 \mu\text{m}$; even for ultrafine particles, the barycentric flow is always the most significant. The length of magnetotactic bacterium was $1 \approx 2 \mu\text{m}$. Thus, the diffusional term could be neglected. Ignoring the effect of diffusion, meanwhile approximately assuming $\epsilon \approx \epsilon_0$, then the Eq. (2) was:

$$u_0 \frac{\partial C}{\partial x} + \frac{\partial (N + \epsilon_0 C)}{\partial t} = 0 \quad (3)$$

Assuming x and t in Eq. (3) were variables, and then the simplified material balance equation could be obtained [18–20]:

$$u_0 \left(\frac{\partial C}{\partial x} \right)_t + \left(\frac{\partial N}{\partial t} \right)_x = 0 \quad (4)$$

3.2. Separation rate equation

In a given time length of δt , the increasing particles mass in the matrix unit was $\left(\frac{\partial N}{\partial t} \right)_x \delta t \cdot \delta x \cdot A$, and the unit input particle mass was $C \cdot u_0 \cdot \delta t \cdot A$, then the trapping probabilities of the particles by metal wire were shown as follows:

$$P = \left(\frac{\partial N}{\partial t} \right)_x \frac{\delta x}{C \cdot u_0} \quad (5)$$

What’s more, in the matrix unit, the length of metal wire was:

$$L_{Tot} = \frac{(1 - \epsilon_0) \cdot \delta x \cdot A}{\pi \cdot a^2} \quad (6)$$

where a was the radius of metal wire.

The effective trapping areas of per-unit length of the metal wire was $2a\pi R_c$, where R_c was the specific trapping radius, then the effective trapping areas (A_{eff}) of the metal wire was:

$$A_{eff} = \frac{(1 - \epsilon_0) \cdot \delta x \cdot A}{\pi \cdot a^2} \cdot 2a\pi R_c = \frac{2(1 - \epsilon_0) \cdot \delta x \cdot A \cdot R_c}{a} \quad (7)$$

Then, the trapping probabilities of particles in the matrix unit by the metal wire were as follows:

$$P = \frac{A_{eff}}{A} = \frac{2(1 - \varepsilon_0) \cdot R_c \cdot \delta x}{a} \quad (8)$$

Assuming Eq. (5) equals to Eq. (8), then:

$$\left(\frac{\partial N}{\partial t} \right)_x = \frac{2(1 - \varepsilon_0) \cdot R_c \cdot u_0 \cdot C}{a} \quad (9)$$

Seen from Eq. (9), the specific trapping radius R_c functional depends on the trapping mass N . Let the specific trapping radius R_c be as follows [21]:

$$R_c = R_{c0} G(N) \quad (10)$$

$$G(N) = \left(1 - \frac{N}{N_t} \right)^\gamma \quad (11)$$

where $G(N)$ was the loss function, and R_{c0} was the critical specific trapping radius. N_t was the maximum trapping amount and γ was the loss constant.

Consequently, the Eq. (9) could be described as follows:

$$\left(\frac{\partial N}{\partial t} \right)_x = \frac{u_0}{L_0} G(N) C \quad (12)$$

where L_0 was the characteristic trapping length and was shown as follows:

$$L_0 = \frac{a}{2(1 - \varepsilon_0) R_{c0}} \quad (13)$$

3.3. Model solution method

In summary, the magnetic separation process could be described by Eqs. (4) and (12), which was a binary first order system of ordinary differential equations, which could be solved by finite element difference method.

The initial conditions and the boundary conditions had to be determined before the solution. The initial conditions could be as follows:

$$\text{when } t = 0, C = N = 0 \quad (0 \leq X \leq L) \quad (14)$$

Under the effect of magnetic field, the solute had the tendency of leaving the solution immediate after the entrance of solution into the separator. However at this starting point, the metal wire had no tendency of adsorbing the solute. Therefore it was needed a certain

time for the movement of solute from bulk solution to the metal wire. The metal wires trapping amount N , from the starting point and along with direction of wire, has a zero local change rate. And the local change rate of concentration in the solution (C) could be solved by the combination of Eqs. (4) and (12):

$$\frac{\partial C}{\partial x} = -\frac{1}{L_0} G(N) C \quad (15)$$

Then the boundary condition at the starting point of the metal wires could be obtained:

$$\text{when } x = 0, \frac{\partial N}{\partial x} = 0, \frac{\partial C}{\partial x} = -\frac{1}{L_0} G(N) C_0$$

This belonged to Neumann boundary condition.

Examining the metal wire, the boundary condition at the end of the metal wires was as follows:

$$\text{when } x = L, \frac{\partial N}{\partial x} = 0, \frac{\partial C}{\partial x} = 0$$

This also was a Neumann boundary condition.

The critical specific trapping radius R_{c0} in the magnetic separation equation was calculated as follows [22]:

$$R_{c0} = \left(\frac{\frac{u_m \cos 2\theta_0}{\frac{\sqrt{2}}{2} + 0.74}}{\frac{u_0}{2}} \right)^{\frac{1}{3}} = 0.8841 \cdot \left(\frac{u_m \cos 2\theta_0}{u_0} \right)^{\frac{1}{3}} \\ = 0.8263 \cdot \left(\frac{u_m}{u_0} \right)^{\frac{1}{3}} \quad (16)$$

where u_m was the characteristic magnetic rate, calculated by:

$$u_m = \frac{2}{9} \frac{\mu_0 (\chi_p - \chi_f) H_0 M_s b^2}{\mu a} \quad (17)$$

where μ was the dynamic viscosity coefficient of the fluid, and u_0 was the flow velocity, b was the radius of particle in solution. θ_0 was the critical trapping angle, which was angle between the particle moving direction and magnetic field line. χ_p and χ_f were the magnetic susceptibility for particles and fluid, respectively. H_0 was the external magnet intensity (i.e., background homogeneous magnet). M_s was the saturated magnetization of the metal wire; μ_0 was the vacuum magnetic permeability.

Table 1
The parameters involved in the magnetic separation mode

Symbol	Value	Source
b	1 μm	measured
a	25 μm	measured
M_s	$1.3 \times 10^6 \text{ A m}^{-1}$	[24]
χ_t	$5 \times 10^{-5} \text{ m}^3 \text{ kg}^{-1}$	[24]
H_0	200 \approx 1200 Gs	measured
μ	$1.01 \times 10^{-3} \text{ Pa s}$	[24]
μ_0	$4\pi \times 10^{-7} \text{ N A}^{-2}$	constant
a	25 μm	measured
$1-\varepsilon_0$	2.45×10^{-5}	measured
γ	$1 \approx 2$	[18]
θ_0	17.6°	[22]
χ_p	$1.01 \times 10^{-3} \text{ m}^3 \text{ kg}^{-1}$	[25]
u_0	0.5 \approx 5 mm s^{-1}	measured
C_0	0.05 \approx 0.5 g l^{-1}	measured

N_T could be calculated by [23]:

$$N_T = \frac{4\theta_0}{2\pi} \times \pi \left[(a \cdot R_{c0})^2 - a^2 \right] \times \frac{A \cdot (1 - \varepsilon_0)}{\pi \cdot b^2} \times C_0 \quad (18)$$

The parameters [18,24,25] needed in the equation calculation were shown in Table 1.

4. Simulation results and discussion

4.1. Simulation results and verification

The accuracy of the model could be examined by the comparison between the experimental data (Exp.) and the calculated results (Cal.) under different magnetic intensity, initial concentration and velocity. The effect of magnetic intensity on the outlet concentration was shown in Fig. 3, in which C/C_0 was the ratio of outlet and original concentration, and the separation efficiency decreased as the rise of the C/C_0 . Also it could be seen from Fig. 3 that the higher the magnetic intensity was, the higher separation efficiency was. However, under different magnetic intensity, the time for a metal wire to reach saturated adsorption did not obviously differ from each other. That was to conclude that the magnetic intensity had little effect on the separation rate. The effect of initial concentration of the solution on the effect of separation was shown in Fig. 4, from which it could be seen the increase of initial concentration reduced the time for a metal wire to reach trapping saturation. The effect of flow velocity on the separation was shown in Fig. 5. It revealed the rise of velocity led to the reduction of magnetic separation efficiency.

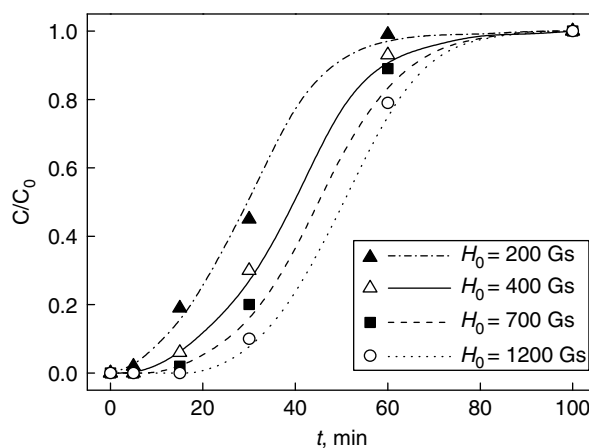


Fig. 3. Effect of the magnetic intensity on separation efficiency ($C_{0,Au} = 80 \text{ mg l}^{-1}$, $u_0 = 1 \text{ mm s}^{-1}$). \blacktriangle , \triangle , \blacksquare , \circ Experimental Data; \cdots , $-$, $---$, \dots Calculated Curves.

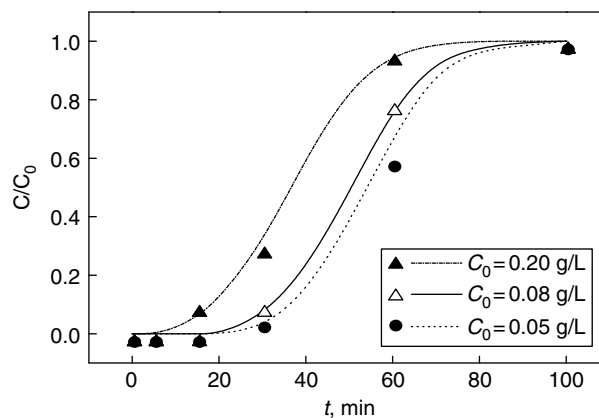


Fig. 4. Effect of initial concentration on separation efficiency ($H_0 = 1200 \text{ Gs}$, $u_0 = 1 \text{ mm s}^{-1}$). \blacktriangle , \triangle , \bullet Experimental Data; \cdots , $-$, \dots Calculated Curves.

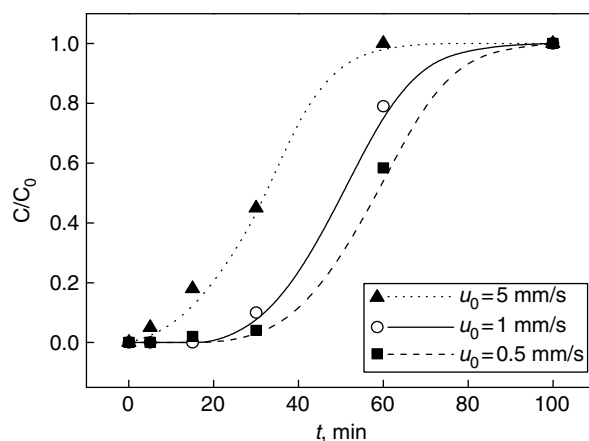


Fig. 5. Effect of the velocity of inlet water on separation efficiency ($H_0 = 1200 \text{ Gs}$, $C_{0,Au} = 80 \text{ mg l}^{-1}$). \blacktriangle , Δ , \blacksquare Experimental Data; \cdots , $-$, $---$, \dots Calculated Curves.

In summary, by the comparison between experimental results and simulated data in Figs. 2–4, the two sets of data were in a good agreement with each other, which indicated the reliability of the model.

4.2. Simulation prediction and experiment results

The model could be used to simulate and predict the magnetic separation process. For instance, the changing trend of the trapping amount with the distance from the inlet after the beginning of magnetic separation was shown in Fig. 6. From Fig. 6 it could be revealed that as the increase of distance and separation time, the trapping amount rose gradually, while the trapping ability (equally the magnetic separation efficiency) decreased step by step, until 100 min it reached saturation.

Taking a magnetic metal wire to exemplify the reason of the separation decrease, assuming the metal wire radius r_a and particles radius r_b , at the initial stage of separation, no particles were trapped by the metal wire, and the high-gradient magnet near the metal surface had strong trapping ability for the particles, having the highest capture potential. After certain time, major surface area of the wire were occupied by particles, and the original metal wire and the trapped particles could be seen as a new wire (having radius $r_a' = r_a + 2r_b$).

The magnetic gradient was in inverse proportion to the metal wire radius. The thinner the wire was, the stronger the promoted magnetic gradient was. Thus, the increase of metal wire radius was larger after trapping process, and the magnetic gradient near the metal surface was weaker. Besides, the magnetic intensity of paramagnetic particles (magnetosomes within MTB) [26,27] was smaller than that of ferromagnetic metal wire. Thus, after the wire absorbed particles the average magnetic

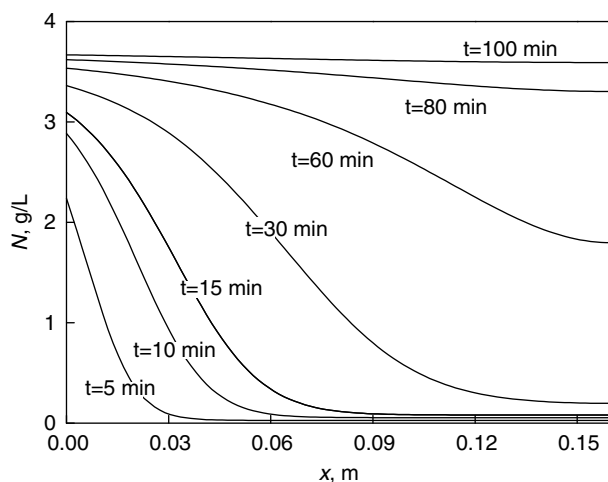


Fig. 6. The trend of trapping amount on the metal wire with distance ($H_0 = 1200$ Gs, $C_{0,Au} = 80$ mg l⁻¹, $u_0 = 1$ mm s⁻¹).

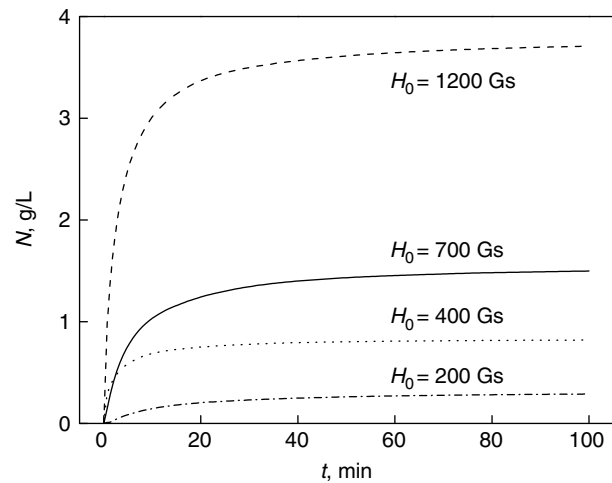


Fig. 7. The trend of trapping amount on metal wire with magnetic field intensity ($C_0 = 80$ mg l⁻¹, $u_0 = 1$ mm s⁻¹).

gradient decreased, which would weaken the magnetic force to the particles in bulk solution and then the separation efficiency.

Analyzed by the model on the separation process, the change of trapping amount with the variance of magnetic intensity could also be shown in Fig. 7, which was in accordance with the results reported in the literature. The increase of magnetic intensity led to the rise of trapping amount, and the metal wire reached saturation at nearly 100 min. It could be seen from Fig. 7 that the saturated trapping amount was proportional to the magnetic intensity, and the scanning electron microscope (SEM) of the MTB-loaded metal wire at different processing time also revealed that the more biomass was adsorbed, the larger the wire radius was, both of which meant the particles were “multi-layer trapped” by the metal wire in the separation process. Such a conclusion could update the previous conception of theoretical research that mainly focused on the behavior of single particle in the magnet, making the theoretical research more close to the fact. Besides, it could be seen that the magnetic intensity had little effect on the separation rate, but large effect on the separation quantity. The higher the magnetic intensity was, the larger the magnetic power was and so did the trapping power of the metal wire.

In the magnetic separation experiment [7], the Au(III) treated biomass was fed into the magnetic separator under different magnetic intensities. Kinetic results showed that after a rapid removal of the biomass in the first 30 min, the rate became level off thereafter, and after 100 min, equilibrium reached (Fig. 8). Also, it can be seen that separation efficiency was proportional to the magnetic intensity, and at the magnetic intensity of 1200 GS, 100% biomass was removed. During the experiment, the nickel wires in the separator were taken

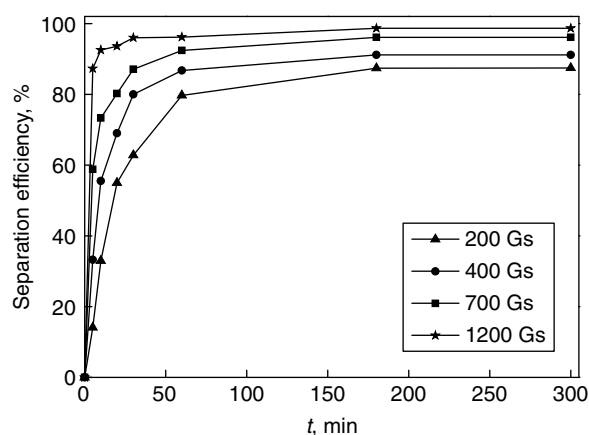


Fig. 8. Separation kinetic study on different magnetic intensities.

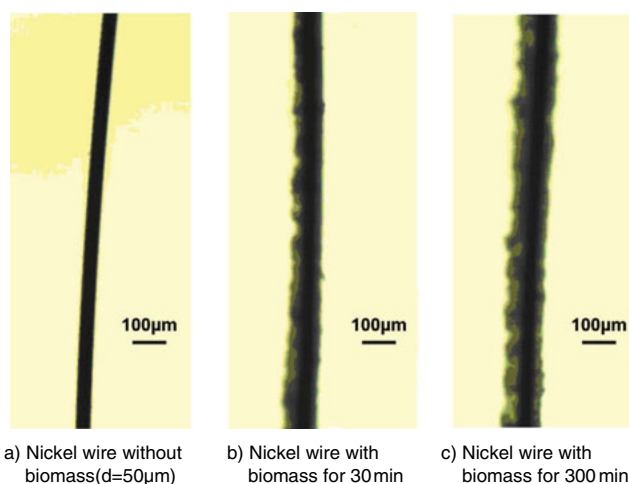


Fig. 9. Micro images of Au loaded biomass on the nickel wires.

out for the observation under the microscopy, and the results showed that the accumulation of MTB biomass on the nickel wires increased with the time (Fig. 9).

Although a laboratory-scale magnetic installation has also been designed for the removal of metal loaded MTB, the measured recovery of the biomass was only 41.7% [6], which significantly limited its application. Apart from the high separation efficiency of the magnetic separator developed in the present study, considering the high biosorption capacity of the magnetotactic biomass and the high gold recovery efficiency of the thiourea, it is possible to apply such an installation into the recovery of Au(III) from industrial wastewater.

5. Conclusions

According to the separation of Au loaded biomass, a model was built on the bases of the material balance equation and separation rate equation. The model was

used to analyze the trapping kinetics characteristics and further to predict the magnetic separation process. The accuracy of the model was investigated by the examination with experimental data under different magnetic intensity, initial concentration and flow velocity, which showed that the magnetic intensity had evident effect on the separation efficiency but obsolete effect on the separation rate of separator. The theoretical simulations results showed that, as the increase of distance from the inlet and the separation time, the trapping amount of the wire also increased, while the trapping ability, namely, the separation efficiency decreased. Another important conclusion was that the bacteria were multi-layer distribution, showing the metal wire had the ability of multi-layer trapping. This model could well match the experimental results, which meant it could be used in the future research of MTB magnetic process.

Acknowledgements

This work was supported by the National Natural Science Foundation of China (No. 20906053 and No.51104097).

Symbols

A	—	lateral area in the separator, m^2
A_{eff}	—	effective trapping areas of the metal wire, m^2
b	—	the radius of particle in solution, $m(\mu m)$
C	—	particle mass content in fluids, $kg\ m^{-3}(g\ l^{-1})$
C_0	—	initial particle mass content in fluids, $kg\ m^{-3}(g\ l^{-1})$
D	—	diffusion coefficient, m^2s^{-1}
$G(N)$	—	loss function, the mathematical statistics term
H_0	—	external magnet intensity Gs
L_0	—	characteristic trapping length, $m(\mu m)$
L_{Tot}	—	length of metal wire, m
M_s	—	saturated magnetization of the metal wire, $A\ m^{-1}$
N	—	adsorbed particle mass for per unit volume of separator, $kg\ m^{-3}(g\ l^{-1})$
N_T	—	maximum trapping amount, $kg\ m^{-3}(g\ l^{-1})$
P	—	trapping probabilities of the particles by metal wire
R_c	—	specific trapping radius, m
R_{c0}	—	critical specific trapping radius, m
t	—	operating time, s
u_0	—	velocity of inlet flow, $m\ s^{-1}(mm\ s^{-1})$
u_m	—	characteristic magnetic rate, $m\ s^{-1}$
x	—	the horizontal distance from the start of the wires
α	—	radius of metal wire, $m(\mu m)$

γ	—	loss constant, the mathematical statistics term
ε	—	porosity of MTB-loaded metal wires
ε_0	—	porosity of clean metal wires
θ_0	—	critical trapping angle
μ	—	dynamic viscosity coefficient of the fluid Pa·s
μ_0	—	permeability of vacuum, $\text{N A}^{-2}(\text{H m}^{-1})$
χ_f	—	magnetic susceptibility for fluid, $\text{m}^3 \text{kg}^{-1}$
χ_p	—	magnetic susceptibility for particles, $\text{m}^3 \text{kg}^{-1}$

Appendix A

Formula derivations of some parameters associated with this paper were listed as follows. (Quote from the sixth chapter of Ref. [22], i.e., PhD thesis of this paper’s author).

When a new magnetic particle was toward the surface of the granular layer on the metal wire, the most stable position should be the location of O point, as shown in Fig. 10 [28]. And the contact points on the four adjacent particles were A_1, A_2, A_3 and A_4 , respectively. Next, the torques in A_2A_4 -axis and A_3A_4 -axis were investigated.

In Fig. 10, F_D was the fluid resistance; F_{Mr} was the radial component of the magnetic force; and A_2A_4 was the distance between point A_2 and point A_4 . The stable condition of the particle in the plane (r - z) was:

$$A_2A_4 \cdot F_{Mr} \geq A_2A_4 \cdot F_D \tag{19}$$

$F_{M\theta}$ was the tangential component of the magnetic force; A_3A_4 is the distance between point A_3 and point A_4 . Similarly, the conditions of torque balance and particle stability in the plane (r - θ) was:

$$A_3A_4 \cdot F_{Mr} \geq A_3A_4 \cdot F_{M\theta} \tag{20}$$

$F_{M\theta}$ and F_{Mr} in (19) and (20) were expressed as [29]:

$$F_{Mr} = \frac{8\pi\mu_0 (\chi_p - \chi_f) H_0 M_s a^2 b^3}{3r^3} \left(K \frac{a^2}{r^2} + \cos 2\theta \right) \tag{21}$$

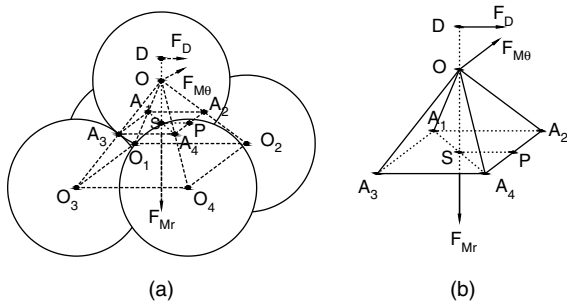


Fig. 10. Stress analysis on the particle on the surface of the wire.

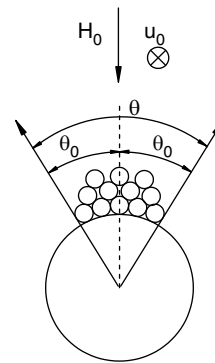


Fig. 11. The schematic layout of the critical trapping angle.

$$F_{M\theta} = \frac{8\pi\mu_0 (\chi_p - \chi_f) H_0 M_s a^2 b^3}{3r^3} \sin 2\theta \tag{22}$$

where a was the wire radius, b the particle radius, r the distance between the wire axis and the particle, χ_p the magnetic susceptibility for particles, χ_f the magnetic susceptibility for fluid, H_0 the external magnet intensity (i.e., background homogeneous magnet), M_s the saturated magnetization of the metal wire, μ_0 the vacuum magnetic permeability, θ_0 the critical trapping angle (i.e., half of the angle θ between the particle moving direction and magnetic field line, in Fig. 11).

The fluid resistance was acting at the point D [30], that is, $0.74 b$ from the center point O. Then, $Sp = PA_4 \frac{b}{2}$, $OS = \frac{\sqrt{2}}{2} b$, $DS = \left(\frac{\sqrt{2}}{2} + 0.74 \right) b$ Formula (21) and (22) were substituted into the formula (19) and (20):

$$F_{Mr} \frac{b}{2} - F_D \left(\frac{\sqrt{2}}{2} + 0.74 \right) b \geq 0 \tag{23}$$

$$K \frac{a^2}{r^2} + \cos 2\theta \geq \sqrt{2} \sin \theta \tag{24}$$

In fact, the particles accumulation status on each wire must satisfy Eqs. (23) and (24). a is the wire radius, r the distance between the wire axis and the particle. So $a < r$. Nickel wires used in this experiment are strong magnetic material (susceptibility $K 6 \times 10^{-6}$ [25]), so the term $K \frac{a^2}{r^2}$ is far less than 1, which can be ignored. Thus, Eq. (24) can be simplified as:

$$\theta \leq \arctg \frac{\sqrt{2}}{2} = 35.3^\circ \tag{25}$$

$$\theta_0 = 0.5 \theta = 17.6^\circ$$

The liquid flow rate is relatively small during the magnetic separation. It belongs to the laminar flow state, that is, ignoring the transverse bending effects of the accumulation surface and the effects of particle gaps on the flow. So, the particle motion was at Stokes region in laminar flow state. The fluid drag force F_D could be calculated by Eq. (26):

$$F_D = 3\pi u_0 dp \mu = 6\pi u_0 b\mu \quad (26)$$

where μ was the dynamic viscosity coefficient of the fluid.

F_{Mr} and F_D were substituted into formula (23):

$$\frac{2\mu_0(\chi_p - \chi_f)H_0M_s a^2 b^2}{9r^3\mu u_0} \left(K \frac{a^2}{r^2} + \cos 2\theta \right) - \left(\frac{\sqrt{2}}{2} + 0.74 \right) \geq 0 \quad (27)$$

where $u_m = \frac{2}{9} \frac{\mu_0(\chi_p - \chi_f)H_0M_s b^2}{\mu a}$ was the characteristic magnetic speed of the particles, $R_c = \frac{r}{a}$ the specific trapping radius for magnetic particles on the wire axis. Thus, Eq. (27) can be simplified as:

$$R_c = \left(\frac{u_m \left(\frac{K}{R_c^2} + \cos 2\theta \right)}{\frac{\sqrt{2}}{2} + 0.74} \right)^{\frac{1}{3}} \quad (28)$$

Since a and r were the same order of magnitude, that is, R_c is similar to 1. $K = 6 \times 10^{-6}$, so the term $\frac{K}{R_c^2}$ is much smaller than 1, which can be ignored. The critical specific trapping radius R_{c0} could be calculated as Eq. (29):

$$R_{c0} = \left(\frac{u_m \cos 2\theta_0}{\frac{\sqrt{2}}{2} + 0.74} \right)^{\frac{1}{3}} = 0.8841 \cdot \left(\frac{u_m \cos 2\theta_0}{u_0} \right)^{\frac{1}{3}} \\ = 0.8263 \cdot \left(\frac{u_m}{u_0} \right)^{\frac{1}{3}} \quad (29)$$

Refer to critical specific trapping radius R_{c0} and the critical trapping angle θ_0 , the collection efficiency of particles would be estimated.

References

- [1] A.H. Sulaymon, S.E. Ebrahim and S.M. Abdullah, Removal of lead, cadmium, and mercury ions using biosorption, *Desalin. Water Treat.*, 24 (2010) 344–352.
- [2] U. Danis, Biosorption of copper(II) from aqueous solutions by *pleurotus cornucopiae*, *Desalin. Water Treat.*, 22 (2010) 117–126.
- [3] R.J.E. Martins, V.J.P. Vilar and R.A.R. Boaventura, Removal of Pb(II) from wastewaters by *fontinalis antipyretica* biomass: experimental study and modelling, *Desalin. Water Treat.*, 20 (2010) 179–188.
- [4] R.B. Frankel, G.C. Papaefthymiou, R.P. Blakemore and W. O'Brien, Fe_3O_4 precipitation in magnetotactic bacteria, *BBA-Mol. Cell Res.*, 763 (1983) 147–159.
- [5] K. Erglis, Q. Wen, V. Ose, A. Zeltins, A. Sharipo, P.A. Janmey and A. Cēbers, Dynamics of magnetotactic bacteria in a rotating magnetic field, *Biophys. J.*, 93 (2007) 402–412.
- [6] A.S. Bahaj, I.W. Croudace, P.A.B. James, F.D. Moeschler and P.E. Warwick, Continuous radionuclide recovery from wastewater using magnetotactic bacteria, *J. Magn. Mater.*, 184 (1998) 241–244.
- [7] H.P. Song, X.G. Li, J.S. Sun, S.M. Xu and X. Han, Application of a magnetotactic bacterium, *Stenotrophomonas* sp. to the removal of Au(III) from contaminated wastewater with a magnetic separator, *Chemosphere*, 72 (2008) 616–621.
- [8] H.P. Song, X.G. Li, J.S. Sun, X.H. Yin, Y.H. Wang and Z.H. Wu, Biosorption equilibrium and kinetics of Au(III) and Cu(II) on magnetotactic bacteria, *Chinese J. Chem. Eng.*, 15 (2007) 847–854.
- [9] T.M. Petrova, L. Fachikov and J. Hristov, The magnetite as adsorbent for some hazardous species from aqueous solutions: a review, *Int. Rev. Chem. Eng.*, 3 (2011) 134–152.
- [10] J.A. Oberteuffer, Magnetic separation: a review of principles, device and applications, *IEEE Trans. Appl. Supercond.*, 10 (1974) 223–238.
- [11] J.H.P. Watson, Theory of capture of particles in magnetic high-intensity filters, *IEEE Trans. Magn.*, 11 (1975) 1597–1599.
- [12] C. Tsouris, J. Noonan, T.Y. Ying and S. Yiaccoumi, Surfactant effects on the mechanism of particle capture in high-gradient magnetic filtration, *Sep. Purif. Technol.*, 51 (2006) 201–209.
- [13] H.T. Chen, M.D. Kaminski and A.J. Rosengart, 2D modeling and preliminary in vitro investigation of a prototype high gradient magnetic separator for biomedical applications, *Med. Eng. Phys.*, 30 (2008) 1–8.
- [14] H.T. Chen, D. Bockenfeld, D. Rempfer, M.D. Kaminski, X.Q. Liu and A.J. Rosengart, Preliminary 3D analysis of a high gradient magnetic separator for biomedical applications, *J. Magn. Mater.*, 320 (2008) 279–284.
- [15] C.T. Yavuz, A. Prakash, J.T. Mayo and V.L. Colvin, Magnetic separations: from steel plants to biotechnology, *Chem. Eng. Sci.*, 64 (2009) 2510–2521.
- [16] G. Iacob, O. Rotariu, N.J.C. Strachan and U.O. Hafeli, Magnetizable needles and wires—modeling an efficient way to target magnetic microspheres in vivo, *Biorheology*, 41 (2004) 599–612.
- [17] J.P. Herzig, D.M. Leclerc, P. Le Goff, Flow of suspensions through porous media—new differential equation for clogged beds is derived, *Ind. Eng. Chem.*, 62 (1970) 8–35.
- [18] Watson, Approximate solutions of the magnetic separator equations, *IEEE T. Magn.*, 14 (1978) 240–245.
- [19] M.R. Parker, Evaluation of magnetic filter performance, *IEEE T. Magn.*, MAG-18 (1982) 822–826.
- [20] R. Gerber and M.H. Watmough, Magnetic separator equations, *IEEE T. Magn.*, MAG-18 (1982) 1671–1673.
- [21] H.H. Kolm, J.A. Oberteuffer and D.R. Kelland, High gradient magnetic separation, *Sci. Am.*, 223 (1978) 47–54.
- [22] H.P. Song, Selective biosorption behavior of precious metal ions on magnetotactic bacteria and gold recovery from gold(III) contained solution, PhD Thesis, Tianjin University, China, 2007 (In Chinese).
- [23] W.G. Peng, Experimental and theory on dust removal with high gradient magnetic separation, Master Thesis, Wuhan University of science and technology, China, 2004 (In Chinese).
- [24] J.H.P. Watson and D.C. Ellwood, Biomagnetic separation and extraction process, *IEEE T. Magn.*, 23 (1987) 3751–3752.
- [25] X.Z. Peng, Paleoclimatic information recorded by microbes and organic matter in Chinese loess—studies on the contributions to the magnetic susceptibility of magnetotactic bacteria

- and the characteristic biomarkers, PhD Thesis. Guangzhou Institute of Geochemistry, Chinese Academy of Sciences, China, 2000 (In Chinese).
- [26] A.H. Li, T. Tang, H.Y. Zhang, Q. Wand, J.S. Tian and Y. Li, Modification of bacterial magnetosomes and application of magnetosome-antibody complex in pathogen detection, *Acta Biophysica. Sinica*, 26 (2010) 680–690.
- [27] B.M. Moskowitz, Biomineralization of magnetic minerals, *Rev. Geophys.*, 33 (1995) 123–128.
- [28] B.S. Zheng, Research on the high gradient magnetic purification mechanism and application technology, PhD Thesis, Institute of Chemical Engineering, South China University of Technology, China, 1997 (In Chinese).
- [29] G. Iacob, A.D. Ciochina and O. Bredetean, High gradient magnetic separation ordered matrices, *Eur. Cell. Mater.*, 3 (2002) 167–169.
- [30] M.E. O'Neill, A sphere in contact with a plane wall in slow linear flow, *Chem. Eng. Sci.*, 23 (1968) 1293.